International Symposium
On Turbulence and Shear Flow
Phenomena (TSFP-9)
June 30 - July 3, 2015 *Melbourne, Australia*

DROPLET DISTRIBUTION AND TRANSPORT IN A TURBULENT SHEAR FLOW

Ali Bagherpour
Department of Mechanical Engineering
University of New Brunswick
15 Dineen Drive, Fredericton, Canada
Ali.Bagherpour@unb.ca

Gordon Holloway
Department of Mechanical Engineering
University of New Brunswick
15 Dineen Drive, Fredericton, Canada
Holloway@unb.ca

INTRODUCTION

Dilute poly-disperse mixtures of liquid droplets and gas phase flow are a common feature of both environmental and technological processes. For example, cloud physics, evaporative humidification and cooling, combustion, surface coating, fire suppression, drug delivery, and pesticide application. Engineering methods for the analysis of such flows are increasingly taking the form of RANS or LES based Computational Fluid Dynamics. However, a recent review of numerical and experimental methods for turbulent dispersed multiphase flow provided by Balachandar & Eaton (2010) draws attention to the need for accurate measurements of size dependent droplet velocities and stresses to evaluate and develop such numerical models. This is especially true for Eulerian methods of droplet transport which offer advantages of computational efficiency and coupling of the droplet phase to the surrounding chemical species such as vapor, oxygen and products of combustion. The transport and concentration field of the droplets depends on the form and scale of the gas-phase turbulence and the droplet inertia. Therefore, the turbulent flow chosen for experimental study should be of practical scale and of a form that emphasizes droplet interaction with sheared turbulence.

In this study a liquid spray dispersed in a disk wake flow is investigated. This type of flow is an idealization of the wake formed behind atomization devices used to introduce droplets into the gas phase. The single phase turbulent wake behind a disk has been studied and turbulence properties of these flows are well characterized in Hinze (1959) and Johansson & George (2006). The two-phase flow, however, has not been studied thoroughly. The emphasis in this work is on the spatial and temporal distribution of droplets and their transport by turbulence according to their size class. The results presented support evaluation and development of Eulerian models of two phase flow.

Gas-phase measurements were conducted using a 3-component Phase Doppler Interferometer (PDI) together with homogeneous seeding using micron size droplets. Hotwire anemometry measurements were performed for purposes of validation. The disk used in the experiment had a diameter, $D = 14cm$, and was made with a sharp beveled edge and streamlined supporting strut. An approach velocity, $\overline{U}_{in} = 68\ m/s$ was used to produce a Reynolds number $Re = U_\infty D/\nu = 6.2 \times 10^5$.

Droplet-phase measurements included droplet size and 3 coincident components of droplet velocity made with the PDI on cross-sections of the spray plume at two positions downwind from the disk, $x/D = 11$ and $x/D = 20$.

MEAN FIELD

Radial profiles of the gas phase axial mean velocity, $\overline{U}_x$, measured with hotwire and PDI in single phase flow are shown in Figure 1. The radial coordinate is normalized by the scale, δ, which is defined in terms of the volumetric flow displacement, $\delta^2 U_0 = \int \left(U_\infty - \overline{U}_x\right) r dr$ where U_0 is the maximum velocity deficit and U_∞ is the free stream axial velocity. For comparison, the experimental data from Johansson & George (2006) are also shown. The scatter in data is mainly due to lack of axisymmetry and the small velocity deficit of the wake which amounts to less than 10% of U_∞. In addition to the mean velocity measurements, radial profiles of Reynolds stress tensor of the gas phase were also measured. The results agreed well with data from axisymmetric single phase wakes described by Johansson & George (2006) and Pope (2008). Radial profiles of mean volume concentration plotted in Figure 1 define the spatial extent of the spray plume.

The droplet size distribution, $f(d)$, shown in Figure 2 was obtained from the shear layer at $x/D = 20$. The majority of droplets had a diameter in the range, $15\mu m < d < 100\mu m$. The total flow rate at each cross section was determined by integrating the volume flux of droplets measured across the spray plume and compared to the total liquid flow rate. The relative error in total volume flow rate was 10.8% at $x/D = 11$ and 16.0% at $x/D = 20$.

In our analysis droplets were grouped into categories based on the Stokes number, $St = \tau_p/\tau_k$, where τ_p is the inertial time scale of the droplets and τ_k is the estimated Kolmogorov time scale of the gas phase turbulence. The time scale of the energy containing gas phase eddies is denoted by τ_e. The range of volume concentration ($C_v < 5 \times 10^{-5}$) and droplet Stokes number ($St_k < 100$) suggest that the interaction of the droplets and the flow can be assumed to have a weak two-way coupling Crowe (2006). This means the interaction between the particles is negligible but the interaction between the particles and flow can affect the turbulence characteristics of the gas phase.

DROPLET STRESSES

A time series of the axial component of droplet velocity, V_x, from the shear layer, $r/\delta = 1$, is plotted in Fig-

ure 3. The record exhibits clusters of droplet arrivals and significant skewness and kurtosis of the velocity. Unlike the homogeneous seeding used to determine the gas phase velocity statistics, the spray droplet distribution is inherently inhomogeneous and considerable care must be taken in the interpretation of its statistics. The arithmetic average of the time series in Figure 3 is considered to be flux weighted (Tropea *et al.* (2007)). In the present work the Reynolds, or ensemble, average was calculated form the velocity records by weighting each velocity by its local inter-arrival time. The Favre average of the droplet velocity, which is used to calculate the turbulent droplet flux, is defined in the present study as

$$\tilde{V} = \frac{1}{T\overline{C_v}} \int_T C_v V dt \tag{1}$$

It was calculated from the velocity records by weighting each droplet velocity by its liquid volume, the inter-arrival time and the inverse of inter-droplet spacing (Bagherpour (2015)). The Reynolds average components of the droplet stress tensor were found to be highly anisotropic. Profiles of droplet velocity covariance, $\overline{v_x v_r}/U_0^2$, are shown in Figure 4. At $x/D = 11$ the values for the droplet phase are comparable to the gas phase shear stress in the shear layer but at $x/D = 20$ the droplet phase covariance has increased substantially whereas the gas phase shear stress has not changed. This trend is even more significant in the correlation coefficient, $\overline{v_x v_r}/v_x' v_r'$, shown in Figure 5. At $x/D = 20$, the values are significantly higher for all the three droplet size classes than the gas phase values.

The particle velocity covariance tensor has been studied using analytical methods by Tchen (1947) and Reeks (2005) who derived analytical expressions for long-time particle velocity covariances in a uniform shear flow. The formula due to Tchen (1947) can be written in the form

$$\frac{\overline{v_i v_j}}{\overline{u_i u_j}} = \frac{K}{(1+\alpha St_e)^n} \tag{2}$$

where $\alpha = \frac{\tau_e}{\tau_L}$ is the ratio of the Eulerian integral time scale of the gas phase turbulence to the Lagrangian time scale, τ_L, of the particle motion and $St_e = \frac{\tau_d}{\tau_e}$. In order to compare the measurements with Tchen's theory average values of the droplet covariance and gas phase stresses were derived from the shear layer ($1 < r/\delta < 1.5$). Since the value of Lagrangian time scale of the droplet motions is not known the value $\alpha \sim 1$ was used. Figure 6 shows that the droplet stresses depend strongly on St_e and are larger than the gas phase stresses for $St_e < 3$. In order to achieve agreement between theory and experiment it was found that $K = 3$ and $n = 2/3$ whereas the theoretical values are $K = 1$ and $n = 1$. The relatively high level of the droplet covariances may be due to the inhomogeneous nature of the flow which affects both sampling and mixing at large scales.

FLUCTUATIONS OF CONCENTRATION

The concentration of droplets is a random field variable that is of considerable importance to modeling droplet transport by the gas phase. However, the concentration field is difficult to measure because of the inherent sample variance of point processes. The droplet distribution in turbulent flows cannot be described as a Homogeneous Poisson Process (HPP), due to both large and small scale clumping of droplets caused by turbulent motions. A more appropriate model of the droplet distribution is a doubly stochastic Poisson process (or Cox process) in which the droplet concentration, C, is a random variable with the mean and variance of $E(C)$ and $var(C)$. The probability of having ΔN droplets in a volume, V, for a Cox process is

$$P(\Delta N, \Gamma) = e^{-\Gamma} \frac{(\Gamma)^{\Delta N}}{\Delta N!} \tag{3}$$

where

$$\Gamma = \int_V C dV \tag{4}$$

is a random variable because the concentration, C, depends on other random physical properties of the flow, e.g. droplet size and velocity. The expected value for the number of droplets in a spatial region, V, is $E(\Delta N) = E(\Gamma)$ and the variance follows from the law of total variance

$$var(\Delta N) = var(\Gamma) + E(\Gamma) \tag{5}$$

It follows from equation 5 that the index of dispersion for a Cox process is larger than one

$$I = \frac{var(\Delta N)}{E(\Delta N)} \geq 1 \tag{6}$$

whereas for an HPP, $I = 1$ since $E(\Delta N) = var(\Delta N) = \Gamma$.

To fit a Cox process to the data an assumption on the distribution of concentration, C, must be made. A distribution that ensures $C > 0$ and is frequently used to model rate events in many applications is the log-normal distribution. To model droplet distribution as an LGCP, a Bayesian method by Vanhatalo *et al.* (2013) was used. Once the pdf is fitted to the data, both the mean concentration field, $\overline{C}$, and its instantaneous deviation from the mean, c, can be determined. For example, the fitted pdf of concentration, C, for the wake centreline is shown in Figure 7.

Using a LGCP fitted to each position in the flow allowed the spatial distribution of variance of the volume concentration, $\overline{c_v^2}$, to be determined. Figure 8 shows radial profiles for 3 categories of Stokes number at $x/D = 20$. The lowest Stokes number having the highest variance of volume concentration relative to its mean centreline concentration. The local intensity, $\frac{c_v'}{\overline{C_v}}$, is very high near the edge of the plume for all Stokes numbers and, where $\overline{C_v}$ is low, it exceeds 100%. The reader is reminded that in spite of the high intensity of fluctuations the concentration is prevented from being negative at any instant because of its log normal distribution.

The variance of concentration fluctuation, $\overline{c_v^2}$, is governed by a balance (Sykes *et al.* (1984)) of production, $P_{\overline{c_v^2}} = -2\overline{v_i c_v}\frac{\partial \overline{C}_v}{\partial x_i}$, and turbulent diffusion. The dominant production term in the present flow is the product of the turbulent flux of concentration in the radial direction and the

radial gradient of mean concentration.The areas of maximum production are roughly aligned with the maxima of the mean concentration gradient. Figures 9 shows the profile of production, $P_{\overline{c_v^2}}$ at axial positions, $x/D = 11$ and 20. The production terms are greatest for droplets in the vicinity of $St = 14$ which is also the size class with the highest relative variance. The peaks of $P_{\overline{c_v^2}}$ are not well aligned with the maxima of $\overline{c_v^2}$ suggesting that turbulent diffusion is significant.

DROPLET CLUSTERING

To study spatial clustering the two-point statistics of the droplet distribution were evaluated using the Pair Correlation Function, or *PCF*. It represents the probability of finding a droplet within distance Δx from a given droplet. This probability is then normalized by the probability of finding a pair of droplets with a Poisson distributed inter-droplet distance Δx with the same mean concentration. Figure 9 shows a sample PCF at $r/\delta = 0.6$ for droplets in 3 categories of St. The spatial separation, Δx, is normalized using the Kolmogorov length scale, l_k. The PCF was derived from PDI measurements using Taylor's frozen turbulence hypothesis so that the smallest measurable droplet separation is the length of the probe volume, l_{pv}, which was in the range of 5-40 times that of the Kolmogorov length scale over the full range of droplet sizes. This imposed filtering effect is a function of droplet diameter as shown in Figure 9. Therefore the shape of PCF in the range $0 < \Delta x/l_k < 40$ should be regarded as an artifact of the measurement.

The PCF shown in Figure 9 has characteristics consistent with a *soft-core process* (Illian *et al.* (2008)), where the maximum, g_{max}, is commonly interpreted as the most frequent inter-droplet distance, $\Delta x_{g_{max}}$. At larger spatial separations than $\Delta x_{g_{max}}$ we have $g(\Delta x) \to 1$ which suggests that it approaches an HPP. It has been shown by Saw *et al.* (2008) that the PCF has the form of a power law function in the range $\Delta x/l_k < 10$ for Stokes numbers in the range $0.01 < St < 1.2$. These works report that the power-law-like region is followed by a plateau region $\Delta x/l_k > 50$, and a decrease at larger separations as observed in the current flow. Other researchers have also found that the PCF is a function of Stokes number and Reynolds number (e.g. Collins & Keswani (2004)).

The spatial extent of droplet clustering in the spray plume is evident in the radial profiles of the maximum value of the PCF, g_{max}, plotted in Figure 10. The values of g_{max} in the shear layer are as high as 10 at $x/D = 20$. A characteristic length scale of the clusters, ζ, can be defined for the pair correlation function of droplets as following

$$\frac{g(\Delta x) - 1}{g(0) - 1} = e^{-\Delta x/\zeta} \tag{7}$$

where, ζ, is an average distance over which the position of two droplets remain correlated. The radial profile of ζ in Figure 11 shows that the scale of droplet aggregation in the wake has a value approximating the integral length scale of the gas phase turbulence, L_e.

Vortex shedding is an important feature of wake flow and it is of interest to evaluate whether it has a significant effect on the droplet cluster formation. The power spectrum of the gas phase velocity in the shear layer shown in (see Figure 12) has a prominent shedding frequency with a Strouhal number, $Sr = 0.15$. Following on the recommendations of Binder & Simpson (2015) for finding clustering scales from a PCF we evaluated the power spectrum of the pair correlation function. The power spectrum of PCF (not shown here) also shows a clear peak at the scales of vortex shedding. These scales were used to calculate the PCF and the results are shown in Figure 13. This suggests that droplet clustering is influenced by the presence of the vortex shedding structures.

TURBULENT DROPLET TRANSPORT

To investigate the effect of the droplet inertia on droplet transport the correlation between radial velocity fluctuations, v_r, and volume concentration fluctuations, c_v, were calculated. This was done using the Favre and Reynolds average of the droplet velocity records obtained from the PDI as

$$\overline{c_v v_r} = \overline{C_v}(\tilde{V} - \overline{V}) \tag{8}$$

Profiles of the correlation coefficient, $\frac{\overline{v_r c}}{v_r' c'}$, in this way at x/D=20 are shown in Figure 14. The correlation coefficients are in the range of $(-0.2, 0.2)$ which is significantly less than one would expect for the correlation coefficient between fluctuations of a passive scalar and velocity in shear flow. The sign of the correlation coefficient in the shear layer has a sign opposite to the local gradient of volume concentration where the latter is a maximum. This is consistent with the common modeling approach in which the turbulent flux is taken as proportional to the gradient of mean concentration with the proportionality being dependent on Stokes number. However, there are also significant regions of negative $\frac{\overline{v_r c}}{v_r' c'}$ near the origin that only partially overlap with the negative gradient of $\overline{C_v}$ near the center of the wake.

In order to evaluate the radial diffusion coefficient, D_{rr}, it was assumed that the flow is axisymmetric and that the gradients in radial direction are much stronger than the axial direction. Using these assumptions

$$D_{rr} = -\overline{v_r c_v}/(\frac{\partial \overline{C}_v}{\partial r}) \tag{9}$$

In presenting the results we follow the common practice of normalizing D_{rr} with the long time estimate of the diffusion coefficient for passive contaminants in homogeneous turbulence, $\tau_{rr}\overline{v_r^2}$. Radial profiles of $D_{rr}/\tau_{rr}\overline{v_r^2}$ are shown in Figure 15 for $x/D = 11$ and 20. The diffusion coefficient varies significantly across the wake in both magnitude and sign; making the validity of a gradient transport model in this inhomogeneous flow questionable.

An estimate of the dependence of $D_{rr}/\tau_{rr}\overline{v_r^2}$ on St_e was made by collecting values near the maximum of the concentration gradient. The results shown in Figure 16 indicate that the diffusion of the droplets depends strongly on St_e and it is nearly zero for the largest droplets in the flow being studied.

References

Bagherpour, A. 2015 Droplet transport in a turbulent wake flow. PhD thesis, University of New Brunswick.

Balachandar, S. & Eaton, J. K. 2010 Turbulent dispersed multiphase flow. *Annual Review of Fluid Mechanics* **42**, 111–133.

Binder, B. J. & Simpson, M. J. 2015 Spectral analysis of pair-correlation bandwidth: application to cell biology images. *Royal Society Open Science* **2** (2), 140494.

Collins, L. R. & Keswani, A. 2004 Reynolds number scaling of particle clustering in turbulent aerosols. *New Journal of Physics* **6** (1), 119.

Crowe, C. T. 2006 *Multiphase flow handbook*. CRC : Taylor & Francis.

Hinze, J. O. 1959 *Turbulence; an introduction to its mechanism and theory*. New York: McGraw-Hill.

Illian, J., Penttinen, A., Stoyan, H. & Stoyan, D. 2008 *Statistical analysis and modelling of spatial point patterns*, , vol. 70. John Wiley & Sons.

Johansson, P. B. V. & George, W. K. 2006 The far downstream evolution of the high-reynolds-number axisymmetric wake behind a disk. part 1. single-point statistics. *Journal of Fluid Mechanics* **555**, 363–385.

Pope, S. B. 2008 *Turbulent flows*. Cambridge Univ. Press.

Reeks, M. W. 2005 On probability density function equations for particle dispersion in a uniform shear flow. *Journal of Fluid Mechanics* **522**, 263–302.

Saw, E. W., Shaw, R. A., Ayyalasomayajula, S., Chuang, P. Y. & Gylfason, A. 2008 Inertial clustering of particles in high-reynolds-number turbulence. *Physical review letters* **100** (21), 214501.

Sykes, R. I., Lewellen, W. S. & Parker, S. F. 1984 A turbulent-transport model for concentration fluctuations and fluxes. *Journal of Fluid Mechanics* **139**, 193–218.

Tchen, C. 1947 *Mean value and correlation problems connected with the motion of small particles suspended in a turbulent fluid*. Martinus Nijhoff, The Hague.

Tropea, C., Foss, J. F. & Yarin, A. L. 2007 *Springer Handbook of Experimental Fluid Mechanics*. Berlin, Heidelberg: Springer Science+Business Media.

Vanhatalo, J., Riihimäki, J., Hartikainen, J., Jylänki, P., Tolvanen, V. & Vehtari, A. 2013 Gpstuff: Bayesian modeling with gaussian processes. *The Journal of Machine Learning Research* **14** (1), 1175–1179.

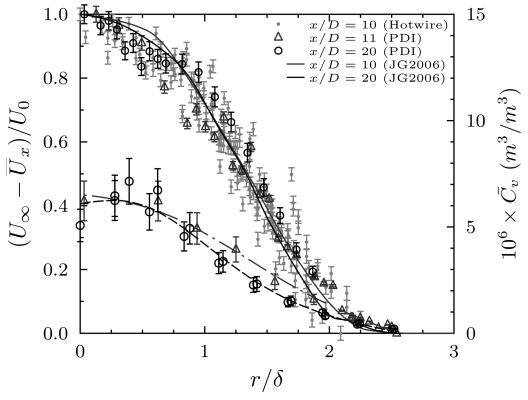

Figure 1. Radial profile of U_0 measured with hotwire and PDI in the wake of the disk at two axial positions. Solid lines show the velocity profiles from Johansson & George (2006). Radial profiles of average volume concentration of liquid spray droplets measured with PDI.

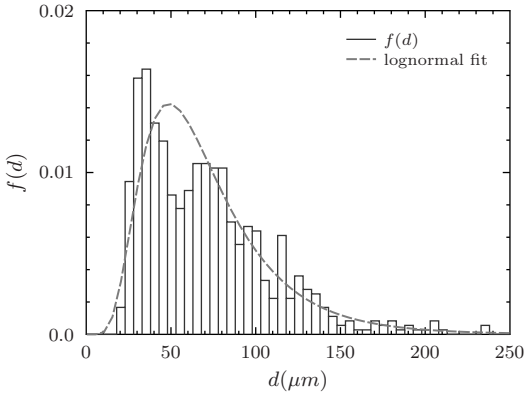

Figure 2. Probability density function, $f(d)$, of droplet size, d, measured in the shear layer at $r/\delta = 1$ and $x/D = 20$. On the wake centreline the shape of $f(d)$ was found to be approximately log-normal.

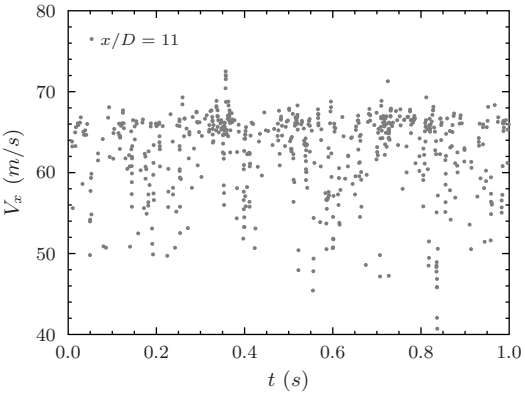

Figure 3. Time series of droplet axial velocity measured in the shear layer of the wake at $x/D = 11$. Record length corresponds to 600 τ_e.

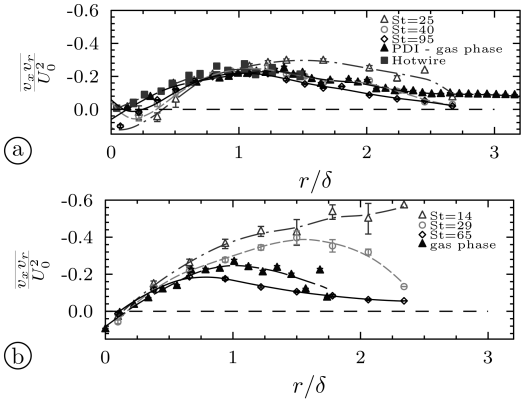

Figure 4. Radial profiles of covariance of the axial and radial droplet velocities at: (a) $x/D = 11$ and (b) $x/D = 20$.

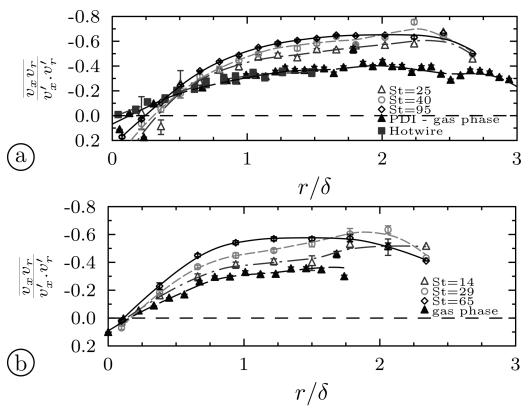

Figure 5. Radial profile of the correlation coefficient between axial and radial droplet velocity at: (a) $x/D = 11$ and (b) $x/D = 20$.

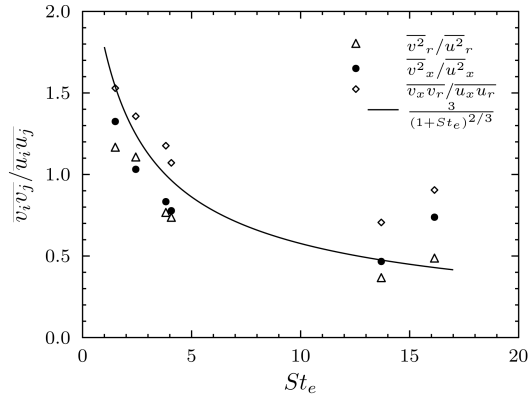

Figure 6. Ratio of the measured components of the droplet stress in the shear layer normalized by the corresponding components of the gas phase Reynolds stress. Solid line represents a modified form of the Tchen (1947) theory for homogeneous turbulence.

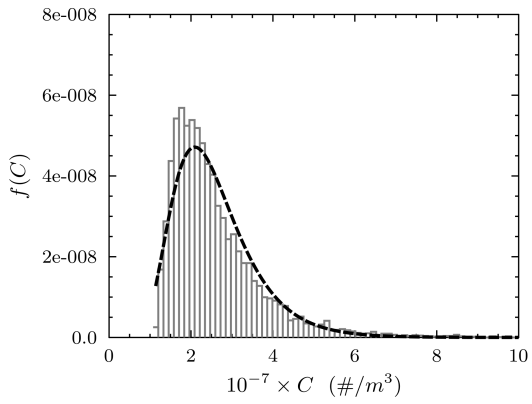

Figure 7. Fitted log-normal Cox Process to the spatial distribution of droplets on the wake centerline at $x/D = 11$.

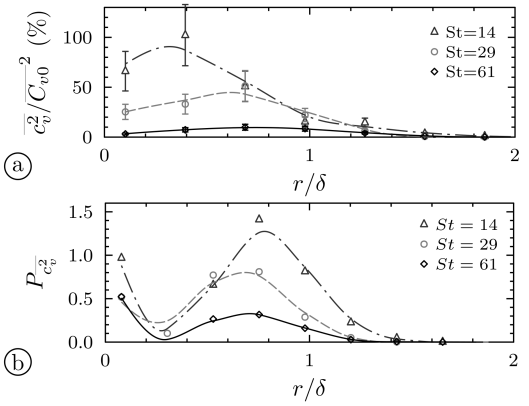

Figure 8. Radial profile of (a) volume concentration variance and (b) production of the concentration variance in the disk wake at $x/D = 20$. $\overline{C_v}_0$ is the centerline value of mean volume concentration for $St = 14$.

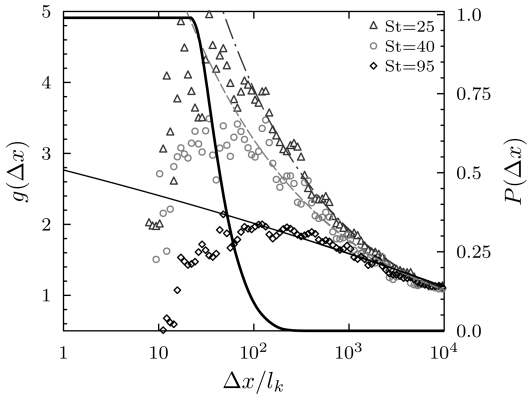

Figure 9. The pair correlation function, $g(\Delta x)$, for 3 categories of Stokes number in the shear layer at $x/D = 11$. The solid thick line, $P(\Delta x)$, shows the probability of rejection of a droplet pair at distance Δx by the PDI instrument. This filtering effect sets the lower limit of Δx for measurement of $g(\Delta x)$ in the present flow.

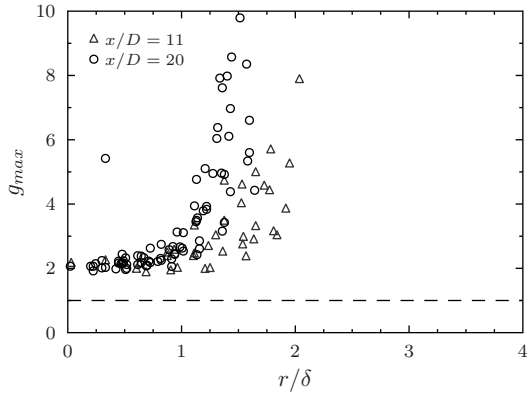

Figure 10. Radial distribution of g_{max} for the entire droplet population at two axial positions. The shear layer is located in the range $1 < r/\delta < 2$.

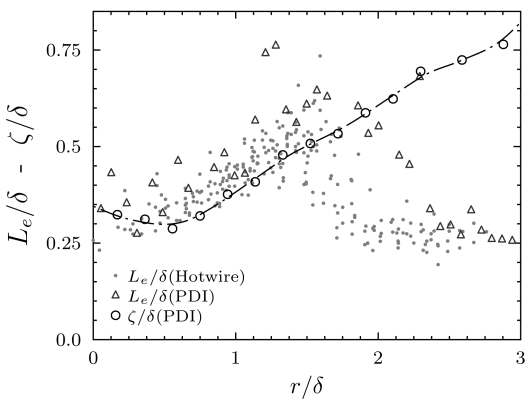

Figure 11. Length scale of the pair correlation function, ζ, compared to the integral length scale of axial gas phase velocity fluctuations , L_e.

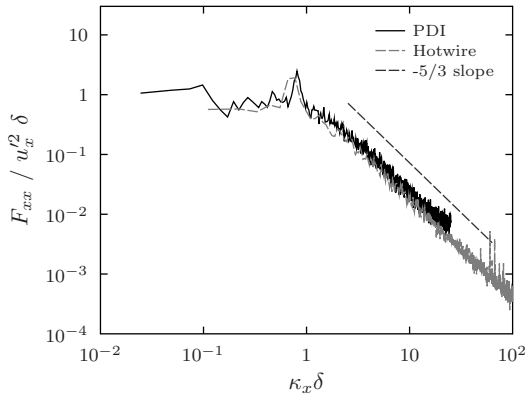

Figure 12. Power spectra of the axial component of gas phase velocity measured by PDI and hotwire at $r/\delta = 1$ and $x/D = 11$.

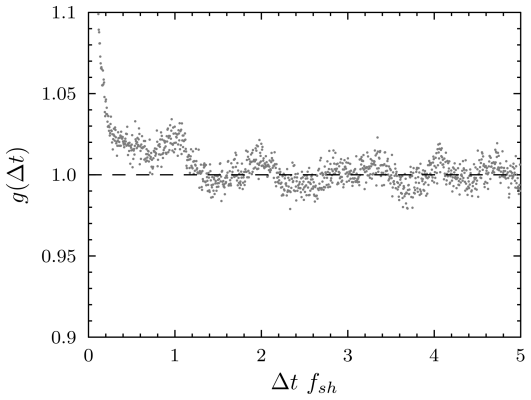

Figure 13. Power spectrum of pair correlation function at $r/\delta = 1$ and $x/D = 11$.

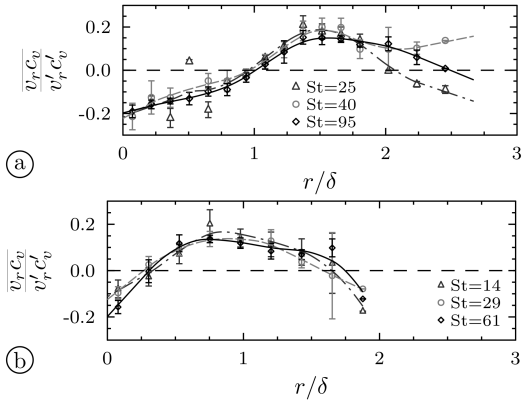

Figure 14. Radial profiles of correlation coefficient, $\overline{v_r c_v}/(v_r' c_v')$, between fluctuations of radial velocity and volume concentration at: (a) $x/D = 11$ and (b) $x/D = 20$.

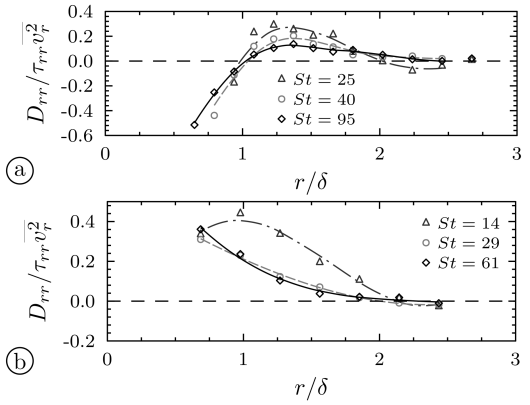

Figure 15. Profiles of the radial coefficient of concentration diffusivity, D_{rr} at: (a) $x/D = 11$ and $x/D = 20$.Values are normalized by the theoretical diffusivity of a passive scalar in homogeneous turbulence.

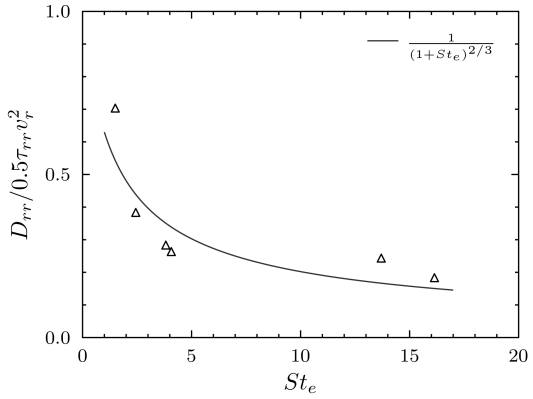

Figure 16. The dependence of the radial component of concentration diffusivity, D_{rr} , on Stokes number. Values measured in the shear layer at $x/D = 11$ and $x/D = 20$.